

02

Softening of lattice modes in the region of structural phase transitions in a composite $\text{Bi}_2(\text{Sn}_{0.7}\text{Fe}_{0.3})_2\text{O}_7/\text{Bi}_2\text{Fe}_4\text{O}_9$

© L.V. Udod^{1,2}, S.S. Aplesnin^{1,2}, M.N. Sitnikov², O.B. Romanova¹, H. Ablebaki²

¹Kirensky Institute of Physics, Federal Research Center KSC Siberian Branch of Russian Academy of Sciences, 660036 Krasnoyarsk, Russia

²Reshetnev Siberian State University of Science and Technologies, 660037 Krasnoyarsk, Russia

e-mail: luba@iph.krasn.ru

Received March 17, 2023

Revised May 25, 2023

Accepted May 29, 2023.

The composite compound $\text{Bi}_2(\text{Sn}_{0.7}\text{Fe}_{0.3})_2\text{O}_7/\text{Bi}_2\text{Fe}_4\text{O}_9$ with a ratio of 91%/9% was obtained by solid-phase synthesis. The mutual influence of two different crystal structures on structural transitions was studied using X-ray diffraction, IR spectroscopy and sound attenuation coefficient. IR absorption spectra were studied in the temperature range 80–500 K and the frequency range 350–7000 cm^{-1} . The types of vibrations of phonon modes are determined. The influence of the $\text{Bi}_2(\text{Sn}_{0.7}\text{Fe}_{0.3})_2\text{O}_7$ matrix on the phonon vibration modes of mullite $\text{Bi}_2\text{Fe}_4\text{O}_9$ was established in the form of a frequency shift $w = 634 \text{ cm}^{-1}$, splitting of the mode $w = 574 \text{ cm}^{-1}$, and disappearance of the mode at the frequency $w = 812 \text{ cm}^{-1}$. In the regions of phase transitions $\text{Bi}_2(\text{Sn}_{0.7}\text{Fe}_{0.3})_2\text{O}_7$ and $\text{Bi}_2\text{Fe}_4\text{O}_9$, a softening of the IR spectra modes was found. The features of the temperature dependence of the sound attenuation

Keywords: composite compound $\text{Bi}_2(\text{Sn}_{0.7}\text{Fe}_{0.3})_2\text{O}_7/\text{Bi}_2\text{Fe}_4\text{O}_9$, phase transitions, IR absorption spectra, phonon modes, sound attenuation.

DOI: 10.61011/EOS.2023.08.57283.4716-23

Introduction

Recently, a direction has emerged in condensed matter physics concerning the study of multiphase systems consisting of compounds with different types of crystal structures and magnetic order [1,2]. Most single-phase materials have a limited scope of applicability. The functionality of materials can be expanded using composites. A combination of several phases, such as a combination of piezomagnetic and piezoelectric or magnetostrictive and piezoelectric phases, can yield a desired property [3]. Such compounds exhibit a number of interesting properties. When the composite contains $\text{Bi}_2\text{Fe}_4\text{O}_9$ and spinel magnetic materials such as MgFe_2O_4 [4], $\text{Bi}_2\text{Fe}_4\text{O}_9/\text{NiFe}_2\text{O}_4$ [5], $\text{Bi}_2\text{Fe}_4\text{O}_9/\text{CoFe}_2\text{O}_4$ [6], they can significantly improve magnetic properties. Magnetoelectric properties are improved by adding CoFe_2O_4 to $\text{Bi}_2\text{Fe}_4\text{O}_9$. Due to the fact that CoFe_2O_4 has high magnetostrictive properties, the voltage will be created by an external field. The created voltage is transferred to the $\text{Bi}_2\text{Fe}_4\text{O}_9$ phase, therefore, piezoelectric properties of $\text{Bi}_2\text{Fe}_4\text{O}_9$ and electrical polarization arise. The increase in magnetization and polarization is associated with the mutual influence of the two structures of the $\text{CoFe}_2\text{O}_4/\text{Bi}_2\text{Fe}_4\text{O}_9$ composite [6]. In the combination of $\text{Bi}_2\text{Fe}_4\text{O}_9$ with barium ferrite as a hard magnetic material, $\text{Bi}_2\text{Fe}_4\text{O}_9/\text{BaFe}_{12}\text{O}_{19}$, the saturation magnetization and the residual magnetization increase due to the increased content of $\text{BaFe}_{12}\text{O}_{19}$. The coercive force increases significantly, even more than that of pure $\text{BaFe}_{12}\text{O}_{19}$ [7]. The magnetiza-

tion of the $x\text{ZnFe}_2\text{O}_4/(1-x)\text{BiFeO}_3$ composite increases greatly with the addition of zinc ferrite concentration. Compounds with $x = 0.3$ and 0.4 show saturated magnetic hysteresis loops with very low coercive force. The anomaly around T_N indicates the magnetoelectric nature of the composite [8]. Nanocomposites containing BiFeO_3 bismuth orthoferrite and $\text{Bi}_2\text{Fe}_4\text{O}_9$ mullite-like ferrite demonstrate an increase in magnetic characteristics compared to pure nanocomposites. This is due to exchange interactions at the interfaces of two phases, ferromagnetic $\text{Bi}_2\text{Fe}_4\text{O}_9$ and antiferromagnetic BiFeO_3 [1,2,9]. Systems consisting of oxides such as BiMnO_3 , BiFeO_3 , and $\text{Bi}_2\text{Fe}_4\text{O}_9$, exhibit a strong connection between ferroelectric and antiferromagnetic properties [10].

Ferroelectricity occurs in materials with no inversion center. The non-centrosymmetric crystal structure includes bismuth pyrostate $\text{Bi}_2\text{Sn}_2\text{O}_7$. At room temperature it belongs to the monoclinic structure (α phase) with space group $P1c1$ [11–13]. The replacement of Sn^{4+} ions with Fe^{3+} ions does not change the space group of the lattice cell symmetry. According to Mössbauer and EPR studies, iron ions in the crystal structure of pyrochlore $\text{Bi}_2(\text{Sn}_{1-x}\text{Fe}_x)_2\text{O}_7$, $x = 0.1, 0.2$, occupy two nonequivalent octahedral positions and are in a high-spin state [14,15]. Temperature dependences of magnetic susceptibility of $\text{Bi}_2(\text{Sn}_{1-x}\text{Fe}_x)_2\text{O}_7$, $x = 0.1, 0.2$, measured in a magnetic field of 600 Oe, look like paramagnetic ones. The paramagnetic Curie temperature increases sharply with increasing concentration of iron ions from $\Theta = -10 \text{ K}$ for $x = 0.1$

to $\Theta_1 = -39.2\text{ K}$ for $x = 0.2$. For the concentration of $x = 0.2$, a decrease is established in the magnetic moment and antiferromagnetic exchange in the region of the structural phase transition from triclinic to monoclinic structure with a change in the anisotropy of exchange at $T = 140\text{ K}$. In bismuth pyrostannate with $x = 0.2$, nonlinear behavior of magnetization in magnetic fields up to 50 kOe was discovered in the paramagnetic state at temperatures up to 200 K , which is associated with the magnetoelectric interaction. The electric polarization induced by a magnetic field is an even function of the magnetic field, except for the region of the structural phase transition, where linear magnetoelectric effect prevails [14,15].

The variety of functional physical properties in pyrochlore compounds (such as ferroelectric [16] and dielectric [17] properties, superconductivity [18,19], oxygen-ion conductivity [20], colossal magnetoresistance [21], absorption of radioactive radiation [22], photocatalysis [23], piezoelectricity [24]) generates a wide interest to these compounds. The connection between the magnetic and electric subsystems in ferroelectromagnets (multiferroics), manifested in the form of magnetoelectric effects, makes it possible to affect the magnetic properties by an electric field. On the other hand, electrical properties of the compounds can be changed by magnetic field. Such compounds have found their application in modern devices for recording and reading information [25,26].

Bismuth ferrite $\text{Bi}_2\text{Fe}_4\text{O}_9$ is an important functional material, which is used as a gas sensor [27] and belongs to the class mullite-like multiferroics [28,29]. It behaves as a paramagnetic at room temperature with an orthorhombic crystal structure $Pbam$ [30]. In the structure of $\text{Bi}_2\text{Fe}_4\text{O}_9$ there are two different positions of the four iron ions Fe^{3+} : $\text{Fe}^{3+}(1)$ occupies the octahedral position of FeO_6 , and $\text{Fe}^{3+}(2)$ occupies the tetrahedral position of Fe_2O_7 [31]. At $T = 264 \pm 3\text{ K}$, bulk $\text{Bi}_2\text{Fe}_4\text{O}_9$ transits to the antiferromagnetic state. The magnetic moment on the Fe^{3+} ion is $\mu = 4.95\mu_B$ [32], according to other data $\mu = 3.9 - 4.0\mu_B$ [33]. The magnetic properties of polycrystalline $\text{Bi}_2\text{Fe}_4\text{O}_9$ depend on the method of production and the size of the crystallites. A sample with a crystallite size of $200\text{--}450\text{ nm}$ [34], synthesized using ethylenediaminetetraacetic acid technology, exhibits weak magnetization at room temperature.

A polycrystal $\text{Bi}_2\text{Fe}_4\text{O}_9$ with micronscale grains, produced by melting, exhibits an antiferromagnetic phase transition at 250 K [35,36]. Polycrystalline ceramics $\text{Bi}_2\text{Fe}_4\text{O}_9$ with a grain size less than 200 nm exhibits magnetic hysteresis at room temperature, which disappears when heated [37]. The critical grain size of 50 nm , at which the magnetization hysteresis appears at room temperature, was found in the $\text{Bi}_2\text{Fe}_4\text{O}_9$ compound produced by the glycine combustion method [38].

Obtaining multiferroic properties in iron-substituted bismuth pyrostanates with long-range magnetic order is a relevant task that can be successfully solved by creating composite compounds. The $\text{Bi}_2(\text{Sn}_{0.7}\text{Fe}_{0.3})_2\text{O}_7/\text{Bi}_2\text{Fe}_4\text{O}_9$

composite with a small content (9%) of mullite exhibits weak ferromagnetism [39]. Residual magnetization of $\text{Bi}_2\text{Fe}_4\text{O}_9$ in the $\text{Bi}_2(\text{Sn}_{0.7}\text{Fe}_{0.3})_2\text{O}_7$ matrix with oxygen deficiency is an order of magnitude higher than the magnetization of pure $\text{Bi}_2\text{Fe}_4\text{O}_9$ polycrystal. The magnetic hysteresis in $\text{Bi}_2(\text{Sn}_{0.7}\text{Fe}_{0.3})_2\text{O}_7/\text{Bi}_2\text{Fe}_4\text{O}_9$ and the lack of magnetization saturation are associated with mullite. To explain the magnetic properties, a model of ferron formation with electron hopping between sublattices from impurity divalent iron ions with absorption of optical magnons is proposed. The magnetic properties of polycrystalline mullite depend on the grain size, which determines the preconditions for the effect on lattice vibration modes.

In multiferroics, the interaction between the magnetic and ferroelectric systems occurs through the crystal lattice. Therefore, studying the crystal structure is important to establish the mechanisms of this interaction.

The purpose of this study is to establish the types of symmetry of the vibrations that are softened in the region of structural and magnetic transitions in the $\text{Bi}_2(\text{Sn}_{0.7}\text{Fe}_{0.3})_2\text{O}_7/\text{Bi}_2\text{Fe}_4\text{O}_9$ composite and dependent on the size of mullite particles.

Experiment

The $\text{Bi}_2(\text{Sn}_{0.7}\text{Fe}_{0.3})_2\text{O}_7/\text{Bi}_2\text{Fe}_4\text{O}_9$ composite was synthesized by the method of solid-phase synthesis with repeated thorough and lengthy intermediate grinding to a homogeneous state in ethyl alcohol. The oxides used as initial materials were „high purity“ Bi_2O_3 , SnO_2 , Fe_2O_3 . The initial mixture of oxides pressed into tablets was placed in a furnace and held at temperatures from 700 to 950°C in the air atmosphere; the holding time ranged from 8 to 24 h .

The powder X-ray diffraction pattern of the synthesized compound was taken using a D8 ADVANCE diffractometer by Bruker at room temperature. The experiment used a VANTEC linear detector and $\text{Cu-K}\alpha$ -radiation. In the X-ray diffraction pattern, in addition to the main monoclinic phase Pc , corresponding to the α -phase of $\text{Bi}_2\text{Sn}_2\text{O}_7$ [40], peaks of $\text{Bi}_2\text{Fe}_4\text{O}_9$ were detected (weight fraction of $\sim 9\%$). Therefore, for the Rietveld refinement, the initial structures of these particular phases were used. However, the coordinates of all 176 atoms of the main phase of $\text{Bi}_2(\text{Sn}_{0.7}\text{Fe}_{0.3})_2\text{O}_7$ were fixed, because their refinement is extremely unstable. The refinement was implemented using the TOPAS 4.2 software [41] and yielded low R-factors of unreliability (Fig. 1).

The crystal structure of $\text{Bi}_2\text{Sn}_2\text{O}_7$ contains 32 ions of Bi^{3+} , 32 ions of Sn^{4+} , and 112 ions of O^{2-} in the independent part of the cell (Fig. 2, *b*). All Bi^{3+} ions have eight O^{2-} ions in their immediate environment and form distorted cubes, and Sn^{4+} are surrounded by six O^{2-} ions and form octahedra, which are connected by vertices.

The crystal lattice of $\text{Bi}_2\text{Fe}_4\text{O}_9$ consists of FeO_6 octahedra arranged parallel to the c axis, connected with double tetrahedra of Fe_2O_7 (Fig. 2, *a*) [39]. The Bi^{3+} ions are

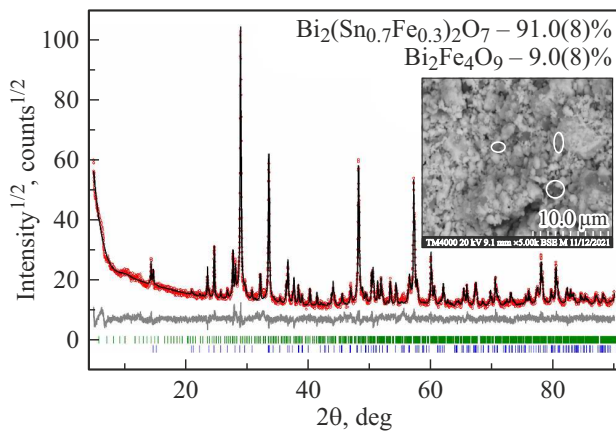


Figure 1. Difference X-ray pattern of $\text{Bi}_2(\text{Sn}_{0.7}\text{Fe}_{0.3})_2\text{O}_7/\text{Bi}_2\text{Fe}_4\text{O}_9$. The inset shows a micrograph of $\text{Bi}_2(\text{Sn}_{0.7}\text{Fe}_{0.3})_2\text{O}_7/\text{Bi}_2\text{Fe}_4\text{O}_9$ and grains of $\text{Bi}_2\text{Fe}_4\text{O}_9$ are highlighted in the form of dark truncated plates with uneven edges.

surrounded by eight oxygen ions with mutually orthogonal short bonds of BiO_3 and longer bonds of BiO_5 [42].

The analysis of microphoto of the $\text{Bi}_2(\text{Sn}_{0.7}\text{Fe}_{0.3})_2\text{O}_7/\text{Bi}_2\text{Fe}_4\text{O}_9$ composite has shown an uneven distribution of $\text{Bi}_2\text{Fe}_4\text{O}_9$ grains (inset in Fig. 1) surrounded by $\text{Bi}_2(\text{Sn}_{0.7}\text{Fe}_{0.3})_2\text{O}_7$ matrix [39]. The $\text{Bi}_2\text{Fe}_4\text{O}_9$ grains are shaped as dark-colored plates with truncated corners and uneven edges. The average grain size of mullite in the bismuth pyrostannate matrix is $1\ \mu\text{m}$ (Fig. 2, c).

It should be noted that optical and acoustic studies are sensitive to local distortions of the structure, therefore the selected methods will provide information on structural phase transitions in $\text{Bi}_2(\text{Sn}_{0.7}\text{Fe}_{0.3})_2\text{O}_7/\text{Bi}_2\text{Fe}_4\text{O}_9$.

The $\text{Bi}_2(\text{Sn}_{0.7}\text{Fe}_{0.3})_2\text{O}_7/\text{Bi}_2\text{Fe}_4\text{O}_9$ was studied by IR absorption spectroscopy using a FSM 2202 IR Fourier spectrometer with a spectral resolution of $1\ \text{cm}^{-1}$ in the temperature range of 80–500 K and a frequency range of $350\text{--}7000\ \text{cm}^{-1}$ with a polycrystalline sample in the form of tablets with a diameter of 13 mm in a KBr matrix.

Acoustic properties were measured directly on the tablets using two piezoelectric sensors glued to the tablet planes with silver paste. One of which was a generator, the other was a receiver of ultrasonic waves. Rectangular pulses with a duration of 100 ns and a frequency of 1 MHz were applied to the piezoelectric sensor; the sample thickness was 0.4 cm. The sound wave attenuation coefficient was calculated by the following formula:

$$\alpha = \frac{1}{d} \ln \left(\frac{U_1}{U_2} \right),$$

where U_1 and U_2 are voltage amplitudes on the generator and receiver of the piezoelectric sensors, d is thickness of the tablet.

The IR absorption spectroscopy

According to X-ray studies, $\text{Bi}_2(\text{Sn}_{0.7}\text{Fe}_{0.3})_2\text{O}_7$ has a pyrochlore structure. The ideal structure of pyrochlore is described by four sets of equivalent points with positional symmetry D_{3d} for cations A and B, C_{3v} for the O anion and T_d for O'. The group-theoretical analysis gives the following distribution of 25 optical modes over irreducible representations:

$$\Gamma_{opt} = A_{1g}(\text{R}) + E_g(\text{R}) + 4F_{2g}(\text{R}) \\ + 7F_{1u}(\text{IR}) + (4F_{2u} + 2F_{1g} + 3A_{2u} + 3E_u).$$

Only 6 of these modes are active in Raman spectra (RS): A_{1g} , E_g , and $4F_{2g}$ and 7 modes are active in IR spectra: $7F_{1u}$ [43,44]. In the IR absorption spectra, both stretching vibrations of oxygen and stretching vibrations of cations A and B appear, and in the Raman spectrum of ideal pyrochlore only vibrational modes of oxygen atoms are observed. Herein, A_{1g} , E_g , and $3F_{2g}$ modes are usually attributed to vibrations of the O-sublattice, and F_{2g} are attributed to vibrations of the O'-sublattice [44]. Thus, in the IR absorption spectra of $\text{Bi}_{3/2}\text{ZnTa}_{3/2}\text{O}_7$, $\text{Bi}_{3/2}\text{MgNb}_{3/2}\text{O}_7$, $\text{Bi}_{3/2}\text{MgTa}_{3/2}\text{O}_7$, $\text{Bi}_{3/2}\text{ZnNb}_{1.52}\text{O}_{6.92}$ bands were found whose frequencies were close to those observed in our study of [45]. The group-theoretical analysis of $\text{Bi}_2\text{Fe}_4\text{O}_9$ includes 14 IR active modes B_{2u} (Table 3 in [46]) and 42 Raman active modes ($12A_g + 12B_{1g} + 9B_{2g} + 9B_{3g}$) [31].

The structural disorder observed in the crystal lattices of bismuth-containing pyrochlores results in a decrease in the positional symmetry of Bi and O atoms, as well as to a violation of the selection rules. Therefore, additional bands may appear in the spectrum of bismuth pyrostannate [44–47].

IR absorption spectra of $\text{Bi}_2(\text{Sn}_{0.7}\text{Fe}_{0.3})_2\text{O}_7/\text{Bi}_2\text{Fe}_4\text{O}_9$ in the frequency range of $350\text{--}1100\ \text{cm}^{-1}$ are shown in Fig. 3 for a number of temperatures. With increasing temperature, an increase in the width of the IR absorption line is observed. A similar behavior of the spectral dependence was observed for $\text{Bi}_2(\text{Sn}_{0.95}\text{Cr}_{0.05})_2\text{O}_7$ [48]. The broadening of absorption lines may be due to the structural positional and orientational disorder and anharmonicity of vibrations. Orientation disorder was discovered in bismuth-containing titanates with a pyrochlore structure, in bismuth oxide and its derivatives [49]. Random orientation of A-O-Bi^{3+} and A-O'-Bi^{3+} electron pairs causes dispersion of vibration frequencies and, accordingly, results in a broadening of the IR absorption spectrum.

The IR spectrum of $\text{Bi}_2(\text{Sn}_{0.7}\text{Fe}_{0.3})_2\text{O}_7/\text{Bi}_2\text{Fe}_4\text{O}_9$ can be conventionally divided into 4 sections in the frequency ranges of 460–510, 510–580, 590–680, 800–1010 cm^{-1} (table). In the frequency range of 460–510 cm^{-1} four modes can be distinguished: 472, 483, 492, and 502 cm^{-1} . The first mode at the frequency of $\omega = 472\ \text{cm}^{-1}$ belongs to stretching vibrations of the Fe-O FeO_6 bond of mullite [50] and the stretching vibrations of the Bi-O' bond in $\text{Bi}_2(\text{Sn}_{0.7}\text{Fe}_{0.3})_2\text{O}_7$ at a frequency of 473 cm^{-1} [43]. The next three modes of 483, 492 and 502 cm^{-1} , correspond

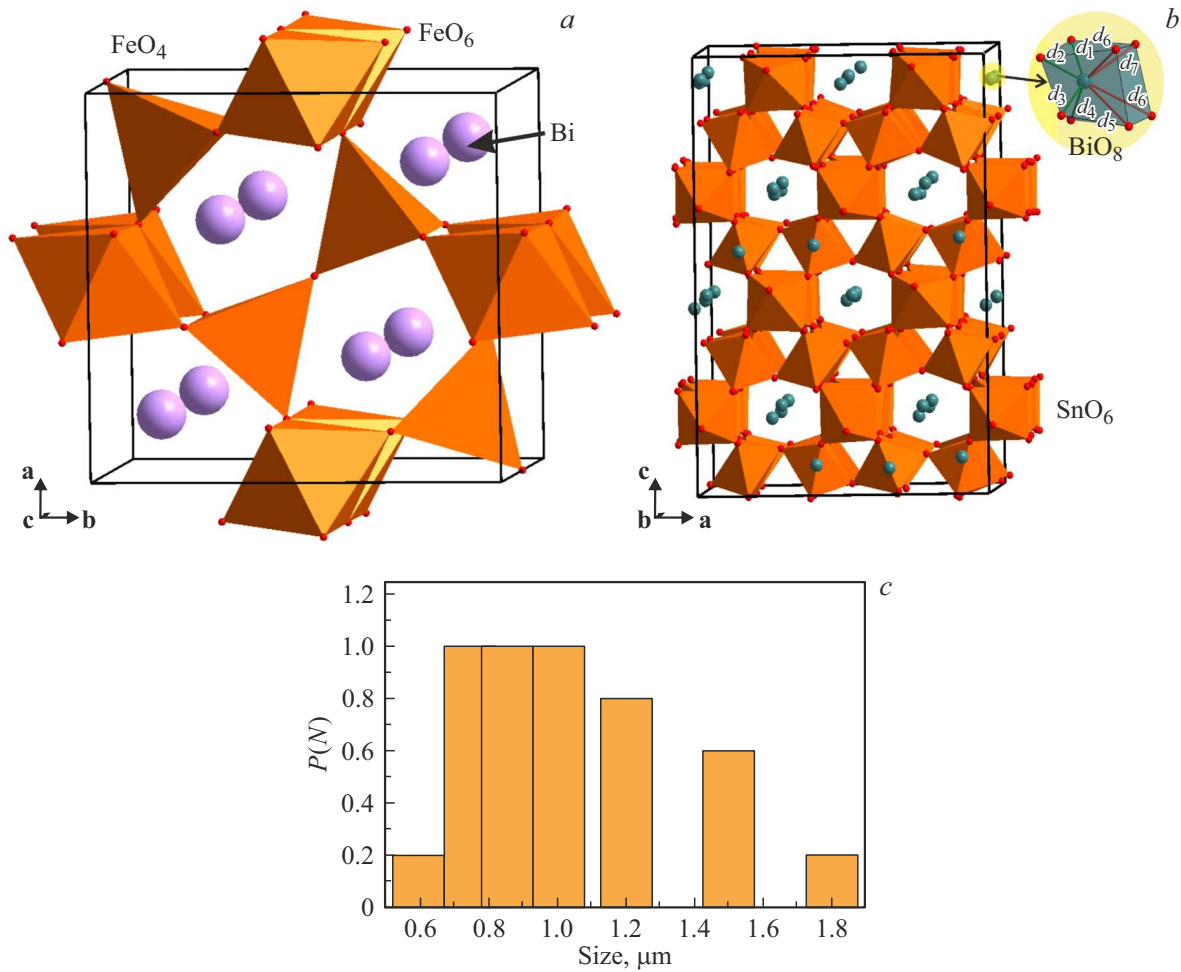


Figure 2. (a) Crystal structure of $\text{Bi}_2\text{Fe}_4\text{O}_9$. (b) Crystal structure of $\text{Bi}_2\text{Sn}_2\text{O}_7$. (c) Grain size distribution in $\text{Bi}_2\text{Fe}_4\text{O}_9$ composite.

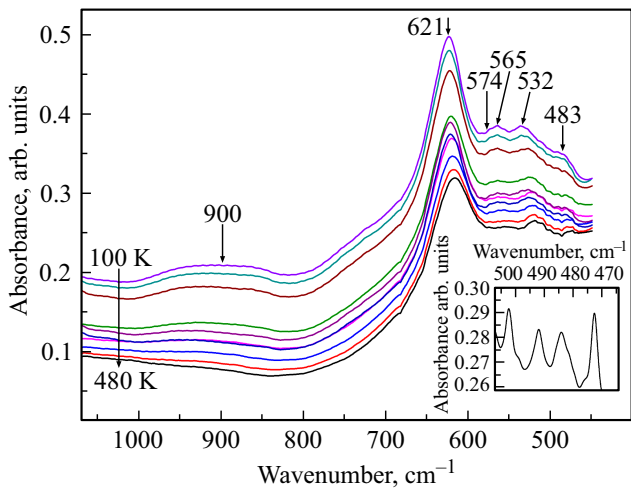


Figure 3. IR absorption spectrum of the $\text{Bi}_2(\text{Sn}_{0.7}\text{Fe}_{0.3})_2\text{O}_7/\text{Bi}_2\text{Fe}_4\text{O}_9$ composite. The inset shows the mode in the frequency region of $\omega = 470 - 510 \text{ cm}^{-1}$.

to the stretching vibrations of the Bi-O' bond in the $\text{Bi}_2(\text{Sn}_{0.7}\text{Fe}_{0.3})_2\text{O}_7$ (Fig. 1, inset on the left). Lines

with close frequencies were detected in cubic pyrochlores $\text{Bi}_{3/2}\text{ZnTa}_{3/2}\text{O}_7$, $\text{Bi}_{3/2}\text{MgNb}_{3/2}\text{O}_7$, $\text{Bi}_{3/2}\text{MgTa}_{3/2}\text{O}_7$, and $\text{Bi}_{3/2}\text{Zn}_{0.92}\text{Nb}_{1.5}\text{O}_{6.92}$ [45]. Lines with frequencies of $\omega = 483, 492 \text{ cm}^{-1}$ belong to stretching vibrations of the Bi-O' [51]. In the crystal structure of $\text{Bi}_2\text{Sn}_2\text{O}_7$ the Sn^{4+} ions occupy nonequivalent crystallographic positions [14,52].

Not all tin ions are replaced by iron. As a result, two types of oxygen octahedra are formed: SnO_6 and FeO_6 . The atomic mass of tin is twice the atomic mass of iron, which results in a distortion of the octahedra containing Fe^{3+} . As a consequence, lengths of the Bi-O' bonds change. This leads to the emergence of spectral lines not previously observed in bismuth pyroostannate. The line at a frequency of 502 cm^{-1} is close to the stretching vibration of the Bi-O' bond in $\text{Bi}_2(\text{Sn}_{0.95}\text{Cr}_{0.05})_2\text{O}_7$ and $\text{Bi}_2\text{Sn}_2\text{O}_7$ [48,53]. In the region of structural phase transitions in $\text{Bi}_2(\text{Sn}_{0.7}\text{Fe}_{0.3})_2\text{O}_7$ at temperatures of $T = 160$ and 400 K the frequencies are softened by 8% (Fig. 4, a). The softening of this line in $\text{Bi}_2(\text{Sn}_{0.7}\text{Fe}_{0.3})_2\text{O}_7/\text{Bi}_2\text{Fe}_4\text{O}_9$ may be caused by distortion of the oxygen octahedron in the crystal lattice of bismuth pyroostannate as a result of doping with iron ions.

Frequencies in the IR absorption spectrum of $\text{Bi}_2(\text{Sn}_{0.7}\text{Fe}_{0.3})_2\text{O}_7/\text{Bi}_2\text{Fe}_4\text{O}_9$ at room temperature

Frequencies of TR modes of $\text{Bi}_2(\text{Sn}_{0.7}\text{Fe}_{0.3})_2\text{O}_7/\text{Bi}_2\text{Fe}_4\text{O}_9$, cm^{-1}	Frequencies of TR modes of $\text{Bi}_2\text{Fe}_4\text{O}_9$, cm^{-1} [50]	$\text{A}_2\text{B}_2\text{O}_7$, cm^{-1}
472	471 Fe-O stretching vibrations (FeO_6)	473 Bi-O' stretching vibrations [43]
483		483 Bi-O' stretching vibrations [51]
492		492 Bi-O' stretching vibrations [51]
502		500 Bi-O' stretching vibrations [43]
519		513 Bi-O stretching vibrations [54]
527		532 O'-vacancy stretching [54]
565	570 Fe-O-Fe bending vibrations (FeO_4)	
574	570 Fe-O-Fe bending vibrations (FeO_4)	
622		625 Sn-O stretching vibrations [43,58]
634	648 Fe-O stretching vibrations (FeO_4)	
	812 Fe-O stretching vibrations (FeO_4)	
900		825 „overtone or combination modes“ [51]

The frequency region of $510\text{--}580\text{ cm}^{-1}$ contains two modes of stretching vibrations (Fig. 4, *b*), which are described by two Lorentz functions with maxima at 519 and 527 cm^{-1} . The line at the frequency of $w = 519\text{ cm}^{-1}$ is close in frequency to the line at $w = 513\text{ cm}^{-1}$ [54] and refers to the stretching vibrations of Bi-O. The frequency of the second line is close to the frequency of the line at $w = 532\text{ cm}^{-1}$ and corresponds to O'-stretching vibrations of the oxygen bond in pyrochlores, known as O'-vacancy stretching (A_{1g}) [53].

A feature of complex bismuth pyrochlores is that, due to the presence of a lone electron pair, the Bi^{3+} ion is displaced from the highly symmetric position $16d$ occupied by cation A in the ideal lattice of pyrochlore, perpendicular to the triple axis to one of six low-symmetry positions $96g(96h)$ [55]. In this case, a displacement of O' takes place and a distortion of the structure, which is referred to as „displacive disorder“ in the literature [56]. The displacement of bismuth atoms leads to rotation of faces of the $\text{Bi}_4\text{O}'$ tetrahedra, stretching of A-O' bonds along the $\langle 110 \rangle$ direction, and displacement of the O' ion from the high-symmetry position $8b$ along the $\langle 111 \rangle$ direction

to one of the four low-symmetry positions $32e$ [57]. At a temperature of 260 K , O'-vacancy stretching ordering apparently occurs at a frequency $w = 527\text{ cm}^{-1}$, which leads to a change in the electron density on the Bi-O' bond.

In the frequency range of $w = 560\text{--}590\text{ cm}^{-1}$ of the IR absorption spectrum of $\text{Bi}_2(\text{Sn}_{0.7}\text{Fe}_{0.3})_2\text{O}_7/\text{Bi}_2\text{Fe}_4\text{O}_9$ there is a mode consisting of two spectral lines at 565 cm^{-1} and 574 cm^{-1} , which are described by the Lorentz function (Fig. 4, *b*). This mode has not previously been observed in bismuth pyrochlores. In $\text{Bi}_2\text{Fe}_4\text{O}_9$ at a frequency of 570 cm^{-1} stretching-bending vibrations of the Fe-O-Fe bond of FeO_4 tetrahedra are observed [50]. The splitting of the mode into two spectral lines is associated with the interaction of two crystal lattices in the composite: Pc for $\text{Bi}_2(\text{Sn}_{0.7}\text{Fe}_{0.3})_2\text{O}_7$ and $Pbam$ for $\text{Bi}_2\text{Fe}_4\text{O}_9$.

The most intense absorption band in the IR spectrum of $\text{Bi}_2(\text{Sn}_{0.7}\text{Fe}_{0.3})_2\text{O}_7/\text{Bi}_2\text{Fe}_4\text{O}_9$ in the frequency range of $590\text{--}680\text{ cm}^{-1}$ with a maximum at 621 cm^{-1} corresponds to the Sn-O stretching vibrations of the oxygen SnO_6 -octahedron [43,58]. Similar mode behavior in this frequency region was observed in $\text{Bi}_2(\text{Sn}_{0.95}\text{Cr}_{0.05})_2\text{O}_7$ [48]. In the same frequency range there are stretching vibrations

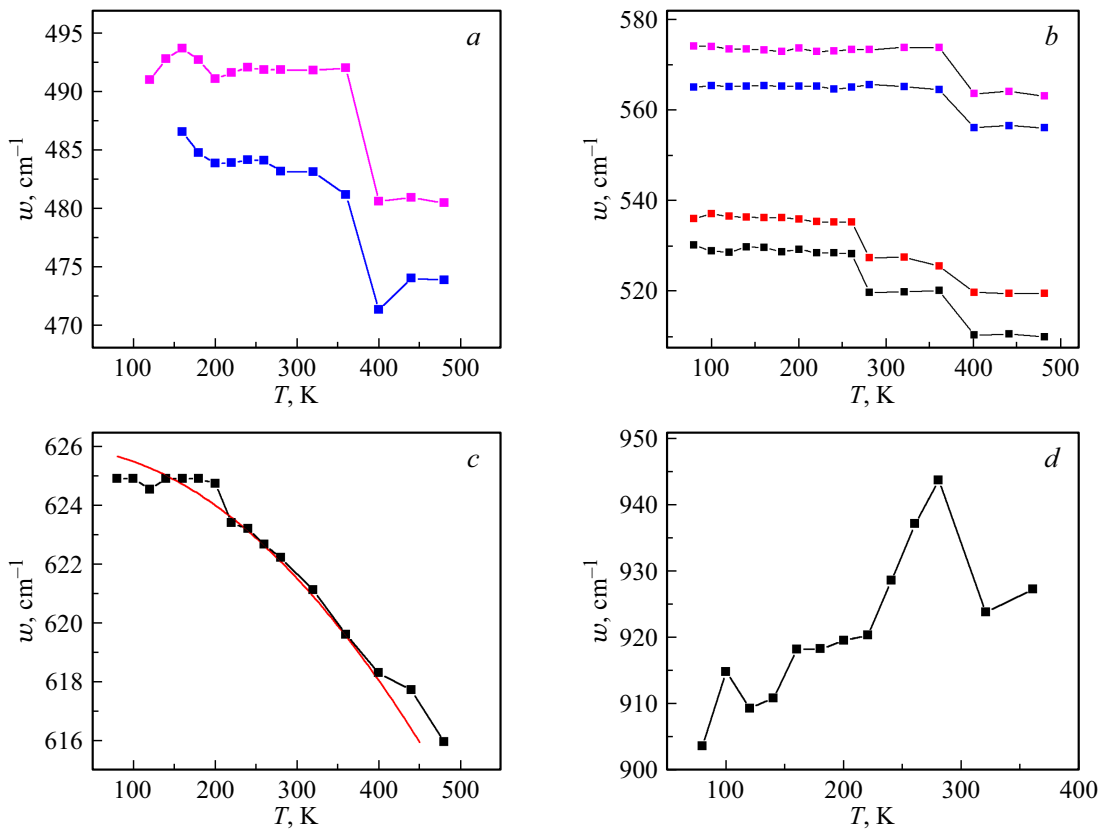


Figure 4. Frequency dependences in the IR absorption spectrum of the $\text{Bi}_2(\text{Sn}_{0.7}\text{Fe}_{0.3})_2\text{O}_7/\text{Bi}_2\text{Fe}_4\text{O}_9$ composite on temperature. For details see the text.

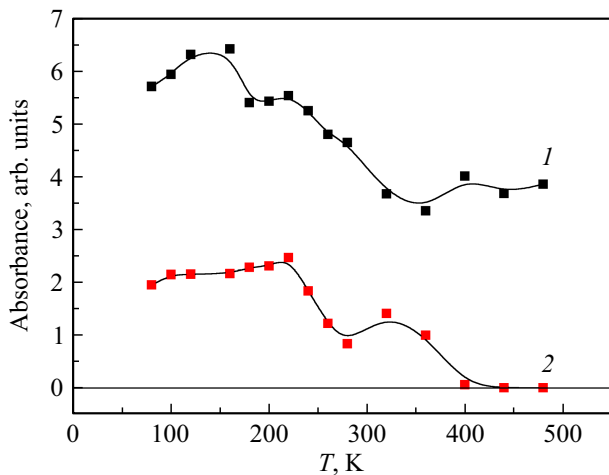


Figure 5. Temperature dependence of mode intensity of $\text{Bi}_2(\text{Sn}_{0.7}\text{Fe}_{0.3})_2\text{O}_7/\text{Bi}_2\text{Fe}_4\text{O}_9$ in frequency ranges: $w = 590 - 680 \text{ cm}^{-1}$ (1) and $800 - 1000 \text{ cm}^{-1}$ (2).

of the Fe-O-group of FeO_4 [50,58]. With increasing temperature, a decrease in the vibration frequency is observed. The intensity of this mode, $w = 590 - 680 \text{ cm}^{-1}$ (Fig. 5, curve 1), has clearly manifested anomalies in the vicinity of structural transitions in bismuth pyrostanate.

The experimental results of the frequency-temperature dependence of this mode are satisfactorily described by the fitting function

$$\omega(T) = \omega_0 + \Delta\omega_{lat} = \frac{\omega_0}{\exp\left(B\left(\frac{T}{T_c}\right)^n\right)},$$

where ω_0 being frequency of harmonic vibrations, $\Delta\omega_{lat}$ being frequency shift as a result of the change in the binding energy of ions both during thermal expansion of the lattice and when the structure of the crystal changes under the effect of deformations or phase transitions. Fitting parameters are: $B = 0.024$, $T_c = 548 \text{ K}$, $n = 2$, $\omega_0 = 626 \text{ cm}^{-1}$. The value of fitting parameter $B = \gamma\alpha_0\Delta T$ is consistent with estimates of existing parameters for oxides: $\gamma = 0.5 - 2$ [59], $\alpha_0 = (2 - 5) \cdot 10^{-5} \text{ K}^{-1}$, $\Delta T = 400 \text{ K}$. Theoretical estimates give for B a range of values of $0.01 - 0.04$. The abrupt change in the intensity of the absorption line at T_c is perhaps due to the appearance of an inversion center in the β -phase of pyrochlore.

At $T = 200 \text{ K}$, a decrease in the mode frequency by 2% is observed, which corresponds to a displacement of the atoms of oxygen octahedra in the direction of one of the crystallographic axes. Similar structural distortions are observed in AXB_3 perovskites [60]. Rotations of octahedra occur in different ways. One possible distortion is the rotation of octahedra around the spatial diagonal ($\varphi\varphi\varphi$),

which leads to a trigonal structure [61]. Superpositions of polar and nonpolar distortions can induce the manifestation of ferroelectric properties along one axis and anti-ferroelectric properties along the other axis. Thus, the analysis of structure of the monoclinic ferroelectric phase in WO_3 and ReO_3 made it possible to detect distortion in oxide systems in the form of a superposition of polar distortion with rotational or antipolar distortion [62]. Rotations of octahedra in WO_3 are combined with the intrinsic anti-ferroelectric displacements of tungsten in the octahedral environment. The resulting structures remain anti-ferroelectric with low spontaneous polarization.

The crystal structure, in addition to the displacement of X ions corresponding to the rotations of soft modes [M] and [R], can allow the displacement of some X ions, as well as A ions. The displacement of ions from equilibrium positions is determined by the minimum potential energy of the entire structure [60]. In this case, the space group may not change.

The complex mode in the frequency range of $800\text{--}1000\text{ cm}^{-1}$ has a wide maximum at $\omega = 900\text{ cm}^{-1}$. In the literature on pyrochlores, this mode is referred to as „overtone or combination modes“. It does not appear in other pyrochlores with an ideal structure [53], arises due to electron-phonon interaction and was observed in $\text{Bi}_2(\text{Sn}_{1-x}\text{Fe}_x)_2\text{O}_7$, $x = 0, 0.1, 0.2$ [63]. In pyrochlore compounds, the mode at a frequency of 850 cm^{-1} [45] corresponds to a change in length of the Bi-O' bond in the $\text{Bi}_2\text{O}'$ sublattice. The difference between long (2.351 \AA) and short (1.961 \AA) bonds is 20%. The displacement of the O' anion and the A cation within the domain results in a shortening of one A-O' bond and a lengthening of the other bond. The line in the frequency range $800\text{--}1010\text{ cm}^{-1}$, which is observed in the IR spectrum of $\text{Bi}_2(\text{Sn}_{0.7}\text{Fe}_{0.3})_2\text{O}_7$, is the sum of two modes, $\omega = 527$ and 417 cm^{-1} , and refers to the stretching vibrations of Bi-O'-bonds.

The intensity of this mode decreases by two times at 270 K (Fig. 5, curve 2). In the region of the structural $\alpha \rightarrow \beta$ -transition of $\text{Bi}_2(\text{Sn}_{0.7}\text{Fe}_{0.3})_2\text{O}_7$ the mode almost disappears. Such changes can be explained by the nonlinearity of elastic properties. In pure mullite, the vibration at a frequency of 812 cm^{-1} is associated with stretching vibrations of oxygen with symmetry A_g and B_{1g} with a weak intensity, which is an order of magnitude lower than the intensity of other vibration modes [31,50]. In the $\text{Bi}_2(\text{Sn}_{0.7}\text{Fe}_{0.3})_2\text{O}_7/\text{Bi}_2\text{Fe}_4\text{O}_9$ composite this line is not observed due to the low concentration of the $\text{Bi}_2\text{Fe}_4\text{O}_9$ compound.

The substitution of tin by iron in bismuth pyrochlore does not change the space group. With an increase in the concentration of Fe^{3+} ions in $\text{Bi}_2(\text{Sn}_{1-x}\text{Fe}_x)_2\text{O}_7$ changes in the IR absorption spectra are observed in the form of broadening, changes in the intensity and frequencies of spectral lines. The decrease in line intensity is most pronounced at frequencies of $\omega = 490\text{--}540\text{ cm}^{-1}$. This frequency region is characterized by vibrations of the Bi-O' bond (F_{1g}) and O'-vacancy stretching (A_{1g}). A four-times decrease in the intensity of the $\omega = 490\text{--}540\text{ cm}^{-1}$

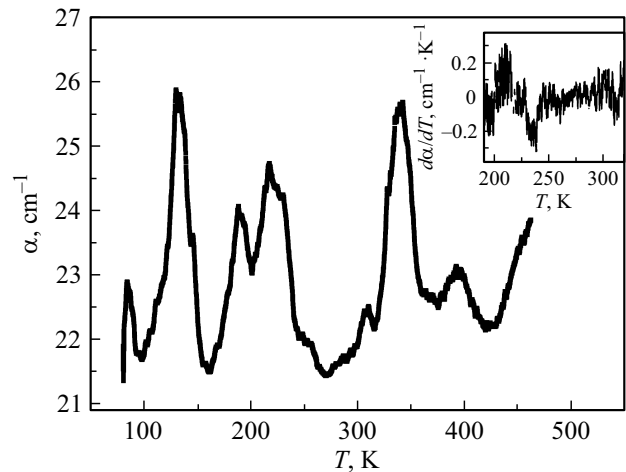


Figure 6. Temperature dependence of the sound attenuation coefficient for $\text{Bi}_2(\text{Sn}_{0.7}\text{Fe}_{0.3})_2\text{O}_7/\text{Bi}_2\text{Fe}_4\text{O}_9$. The inset shows the derivative of the sound attenuation coefficient as a function of temperature.

mode in the IR absorption spectrum of $\text{Bi}_2(\text{Sn}_{1-x}\text{Fe}_x)_2\text{O}_7$ $x = 0.3$ compared to $x = 0, 0.1, 0.2$ is indicative of a decrease in the polarity of the Bi - O' bond and the lone pair effect of the Bi^{3+} ion.

Sound

The temperatures of structural transitions can be determined from the ultrasonic attenuation coefficient. Temperature dependence of the sound attenuation coefficient for the $\text{Bi}_2(\text{Sn}_{0.7}\text{Fe}_{0.3})_2\text{O}_7/\text{Bi}_2\text{Fe}_4\text{O}_9$ composite compound (Fig. 6) has a number of anomalies that correlate with the data for $\text{Bi}_2(\text{Sn}_{1-x}\text{Fe}_x)_2\text{O}_7$, $x = 0.1$ and 0.2 . The first large peak at $T = 130\text{ K}$ is associated with anomalies in the temperature-frequency dependence of the IR spectra. In particular, the vibration mode of SnO_6 -octahedron with $\omega = 625\text{ cm}^{-1}$ softens in frequency at $T = 120\text{ K}$. This anomaly in the temperature dependence of the sound attenuation coefficient is caused by a structural phase transition from a triclinic to a monoclinic crystal structure, which was found in $\text{Bi}_2(\text{Sn}_{1-x}\text{Fe}_x)_2\text{O}_7$, $x = 0.2$ [63].

Anomalies at $T = 190$ and 216 K correspond to changes in the temperature-frequency dependence and intensity of the $\omega = 625\text{ cm}^{-1}$ mode of SnO_6 -octahedron vibration at 200 K in $\text{Bi}_2(\text{Sn}_{0.7}\text{Fe}_{0.3})_2\text{O}_7$. According to Mössbauer spectroscopy data [14], the Sn^{4+} ions occupy two crystallographic positions in the structure of $\text{Bi}_2\text{Sn}_2\text{O}_7$. Apparently, the rotation of oxygen octahedra occurs in two stages: first, octahedra of one type undergo rotational distortions, and at $T = 216\text{ K}$ octahedra of another type are distorted. The distortion of octahedra is sometimes considered as secondary effects of decompensation of antipolar displacements during rotational distortions [60]. It can be assumed that the rotational distortion of oxygen octahedra induces a magnetoelectric effect in $\text{Bi}_2(\text{Sn}_{1-x}\text{Fe}_x)_2\text{O}_7$, $x = 0.2$ [63].

At $T = 200$ K, a nonlinear behavior of magnetization in the paramagnetic state is observed, which is due to the linear magnetoelectric effect

The anomalies at $T = 340$ and 390 K correspond to the $\alpha \rightarrow \beta$ -transition in bismuth pyrostannate. The base compound $\text{Bi}_2\text{Sn}_2\text{O}_7$ has a domain structure and the $\alpha \rightarrow \beta$ -transition occurs in the region of $T = 400$ K [11], and in $\text{Bi}_2(\text{Sn}_{0.8}\text{Fe}_{0.2})_2\text{O}_7$ it starts at $T = 350$ K [63]. Some of the domains containing iron ions begin to rearrange at $T = 340$ K, and at $T = 390$ K the entire sample transits into a single-phase state, the β -phase. At $T = 350$ K, the energy absorption is caused by scattering at domain boundaries, and at $T = 390$ K, the scattering is due to a structural transition. With an increase in the concentration of iron ions, additional maxima appear on the temperature dependence of the sound attenuation coefficient associated with rotational distortions of octahedra [63]. Also, the temperatures of phase transitions from triclinic phase to monoclinic phase and the $\alpha \rightarrow \beta$ transition shift towards low temperatures. The increase in the sound attenuation coefficient above 420 K is perhaps associated with a phase transition to the centrosymmetric structure of bismuth pyrostannate at 548 K. In the region of the magnetic phase transition in mullite at a temperature of 240 K, the rate of ultrasound attenuation with temperature changes sharply (inset in Fig. 6).

Conclusions

In the $\text{Bi}_2(\text{Sn}_{0.7}\text{Fe}_{0.3})_2\text{O}_7/\text{Bi}_2\text{Fe}_4\text{O}_9$ composite vibration modes corresponding to bending and stretching vibrations of mullite have been established. Frequency shift of these modes is associated with the effect of the bismuth pyrostannate matrix.

In the region of structural transitions, a decrease in the frequency of phonon modes was detected, associated with stretching vibrations of the Fe-O bond and with rotational distortion of the SnO_6 octahedra, which provide the prerequisites for the existence of ferroelectric properties.

A decrease in the mode frequency was established at frequencies of $\omega = 519$ and 527 cm^{-1} , related to O' -vacancy stretching (A_{1g}), below room temperature.

In the region of the $\alpha \rightarrow \beta$ — transition, the disappearance of the composite mode was detected, associated with a decrease in nonlinear effects of the lattice.

A sharp decrease in the rate of ultrasound attenuation in the region of the magnetic phase transition in mullite was found.

Funding

The study was carried out within the framework of the research topic of the State Assignment of the Institute of Physics of the Siberian Branch of the Russian Academy of Sciences.

Conflict of interest

The authors declare that they have no conflict of interest.

References

- [1] T. Maity, S. Goswami, D. Bhattacharya, S. Roy. *Phys. Rev. Lett.*, **110** (10), 107201 (2013). DOI: 10.1103/PhysRevLett.110.107201
- [2] T. Maity, S. Roy. *J. Magn. Magn. Mater.*, **494**, 165783 (2020). DOI: 10.1016/j.jmmm.2019.165783
- [3] Jungho Ryu, Shashank Priya, Kenji Uchino, Hyoun-ee Kim. *J. Electroceramics*, **8**, 107 (2002). DOI: 10.1023/A:1020599728432
- [4] L.G. Wang, G.B. Yu, C.M. Zhu, F.Z. Lv, F.C. Liu, W.J. Kong. *J. Mater. Sci. Mater. Electron.*, **30**, 20556 (2019). DOI: 10.1007/s10854-019-02460-0
- [5] Y. Lin, P. Kang, H. Yang, G. Zhang, Z. Gou. *Powder Technol.*, **284**, 143 (2015). DOI: 10.1016/j.powtec.2015.04.072
- [6] M. Salami, O. Mirzaee, A. Honarbakhsh-Raouf, S.A.N.A. Lavasani, A.K. Moghadam. *Ceram. Int.*, **43**, 14701 (2017). DOI: 10.1016/j.ceramint.2017.07.199
- [7] Z.Y. Gao, Y.P. Pu, J. Wei, M.T. Yao, Q. Jin, H.Y. Zheng, Y.R. Wang. *Phys. Status Solidi*, **213**, 2741 (2016). DOI: 10.1002/pssa.201600225
- [8] Poonam Uniyal, K.L. Yadav. *J. Alloys and Compounds*, **492**, 406 (2010). DOI: 10.1016/j.jallcom.2009.10.275
- [9] Panda Alaka, Ramanujan Govindaraj. *Condens. Matter*, **3**, 44 (2018). DOI: 10.3390/condmat3040044
- [10] C.N.R. Rao, A. Sundaresan, R. Saha. *J. Phys. Chem. Lett.*, **3**, 2237 (2012). DOI: 10.1021/jz300688b
- [11] R.D. Shannon, J.D. Bierlein, J.L. Gillson, G.A. Jones, A.W. Sleight. *J. Phys. Chem. Solids*, **41**, 117 (1980). DOI: 10.1016/0022-3697(80)90041-4
- [12] A. Walsh, G.W. Watson. *Chem. Mater.*, **19**, 5158 (2007). DOI: 10.1021/cm0714279
- [13] L.V. Udod, S.S. Aplesnin, M.N. Sitnikov, M.S. Molokeev. *FTT*, **56**, 1315 (2014). DOI: 10.1134/S1063783414070336
- [14] L. Udod, S. Aplesnin, M. Sitnikov, O. Romanova, O. Bayukov, A. Vorotinov, D. Velikanov, G. Patr. *EPJP*, **135**, Article number: 776 (2020). DOI: 10.1140/epjp/s13360-020-00781-2
- [15] S.S. Aplesnin, L.V. Udod, M.N. Sitnikov, O.B. Romanova. *Ceramics International*, **47** (2), 1704 (2021). DOI: 10.1016/j.ceramint.2020.08.287
- [16] W.R. Cook, Jr., H. Jaffe. *Phys. Rev.*, **88**, 1426 (1952). DOI: 10.1103/PhysRev.88.1426
- [17] E. Buixaderas, S. Kamba, J. Petzelt. *Ferroelectrics*, **308**, 131 (2004). DOI: 10.1080/00150190490508909
- [18] M. Hanawa, Y. Muraoka, T. Tayama, T. Sakakibara, J. Yamamura, Z. Hiroi. *Phys. Rev. Lett.*, **87**, 187001 (2001). DOI: 10.1103/PhysRevLett.87.187001
- [19] A.W. Sleight, J.L. Gillson. *Mater. Res. Bull.*, **6**, 781 (1971). DOI: 10.1016/0025-5408(71)90114-0
- [20] M.P. van Dijk, K.J. de Vries, A.J. Burggraaf. *Solid State Ionics*, **9–10**, 913–920 (1983).
- [21] M.A. Subramanian, B.H. Toby, A.P. Ramirez, W.J. Marshall, A.W. Sleight, G.H. Kwei. *Science*, **273**, 81 (1996). DOI: 10.1126/science.273.5271.81
- [22] N.P. Laverov, S.V. Yudintsev, T.S. Livshits, S.V. Stefanovsky, A.N. Lukinykh, R.C. Ewing. *Geochem. Int.*, **48**, 1 (2010). DOI: 10.1134/s0016702910010015

- [23] O. Merka, D.W. Bahnemann, M. Wark. *Catal. Today*, **225**, 102 (2013). DOI: 10.1016/j.cattod.2013.09.009
- [24] S. Kamba, V. Porokhonsky, A. Pashkin, A. Pashkin, V. Bovtun, J. Petzelt, J.C. Nino, S. Trolrier-McKinstry, M.T. Lanagan, C.A. Randall. *Phys. Rev. B*, **66**, 054106 (2002). DOI: 10.1016/S0955-2219(96)00187-2
- [25] G. Catalan, J.F. Scott. *Adv. Mater.*, **21**, 2463 (2009). DOI: 10.1002/adma.200802849
- [26] A.P. Pyatakov, A.K. Zvezdin, *UFN*, **182** (6), 593 (2012) (in Russian). DOI: 10.3367/UFNr.0182.201206b.0593
- [27] Y.A. Park, K.M. Song, K.D. Lee, C.J. Won, N. Hur. *Appl. Phys. Lett.*, **96**, 092506 (2010). DOI: 10.1063/1.3339880
- [28] D.P. Dutta, C. Sudakar, P.S.V. Mocherla, B.P. Mandal, O.D. Jayakumar, A.K. Tyagi. *Mater. Chem. Phys.*, **135**, 998e1004 (2012). DOI: 10.1016/j.matchemphys.2012.06.005
- [29] M. Zhang, H. Yang, T. Xian, Z.Q. Wei, J.L. Jiang, Y.C. Feng, X.Q. Liu. *J. Alloys Compd.*, **509**, 809 (2011). DOI: 10.1016/j.jallcom.2010.09.097
- [30] A. Kirsch, M.M. Murshed, F.J. Litterst, T.M. Gesing. *J. Phys. Chem. C*, **123** (5), 3161 (2019). DOI: 10.1021/ACS.jpcc.8B09698
- [31] M.N. Iliiev, A.P. Litvinchuk, V.G. Hadjiev, M.M. Gospodinov, V. Skumryev, E. Ressouche. *Phys. Rev. B*, **81**, 024302 (2010). DOI: 10.1103/PhysRevB.81.024302
- [32] N. Shamir, E. Gurewitz, H. Shaked. *Acta Crystallogr. A*, **34**, 662 (1978). DOI:10.1107/S0567739478001412
- [33] Z. Pchelkina, S. Streltsov. *Phys. Rev. B*, **88**, 054424 (2013). DOI: 10.1103/PhysRevB.88.054424
- [34] J. Zhao, T. Liu, Y. Xu, Y. He, W. Chen. *Chem. Phys.*, **128**, 388–391 (2011). DOI: 10.1016/j.matchemphys.2011.03.011
- [35] S. Brown, H.C. Gupta, J.A. Alonso, M.J. Martínez-Lope. *Phys. Rev. B*, **69**, (2004) 054434-6. DOI:10.1103/PhysRevB.69.054434
- [36] N.A. Hill. *Annu. Rev. Mater. Res.*, **32**, 1 (2002). DOI: 10.1146/annurev.matsci.32.101901.152309
- [37] M. Roy, InduBala, S.K. Barbar. *J. Therm. Anal. Calorim.*, **110**, 559 (2012). DOI: 10.1007/s10973-012-2525-x.
- [38] X. Wu, J. Miao, Y. Zhao, X. Meng, X. Xu, S. Wang, Y. Jiang. *Optoelectr. Adv. Mater. -RAPID Commun.*, **7**, 116 (2013).
- [39] S.S. Aplesnin, L.V. Udod, M.N. Sitnikov, D.A. Velikanov, M.N. Molokeev, O.B. Romanova, A.V. Shabanov. *JMMM*, **559**, 169530 (2022). DOI: 10.1016/j.jmmm.2022.169530
- [40] I.R. Evans, J.A.K. Howard, J.S.O. Evans. *J. Mater. Chem.*, **13**(9), 2098 (2003). DOI: 10.1039/B305211G
- [41] Bruker AXS TOPAS V4: General profile and structure analysis software for powder diffraction data. — User's Manual. Bruker AXS, Karlsruhe, Germany, 2008.
- [42] Manish Kumar Verma, Vinod Kumar, Tapas Das, Ravi Kumar Sonwani, Vishnu Shankar Rai, Dinesh Prajapati, Kedar Sahoo, Vishal Kumar Kushwaha, Asha Gupta, Kamdeo Mandal. *J. Minerals and Materials Characterization and Eng.*, **9**, 444 (2021). DOI: 10.4236/jmmce.2021.95030
- [43] M.A. Subramanian, G. Aravamudan, G.V. Subba Rao. *Prog. Solid State Chem.*, **15**, 55 (1983). DOI: 10.1016/0079-6786(83)90001-8
- [44] H.C. Gupta, S. Brown, N. Rani, V.B. Gohel, J. Raman Spectrosc., **32**, 41 (2001). DOI: 10.1002/1097-4555(200101)32:1;41::AID-JRS664;3.0.CO;2-R
- [45] M. Chen, D.B. Tanner, J.C. Nino. *Phys. Rev. B*, **72**, 054303 (2005). DOI: 10.1103/PhysRevB.72.054303
- [46] M. Verseils, A.P. Litvinchuk, J.-B. Brubach, P. Roy, K. Beauvois, E. Ressouche, V. Skumryev, M. Gospodinov, V. Simonet, S. de Brion. *Phys. Rev. B*, **103**, 174403 (2021). DOI: 10.1103/PhysRevB.103.174403
- [47] D.J. Arenas, L.V. Gasparov, W. Qiu, J.C. Nino, C.P.D. Tanner. *Phys. Rev. B*, **82**, 214302 (2010). DOI: 10.1103/PhysRevB.82.214302
- [48] S.S. Aplesnin, L.V. Udod, M.N. Sitnikov, N.P. Shestakov. *Ceram. Int.*, **42**, 5177 (2016). DOI: 10.1016/j.ceramint.2015.12.040
- [49] R.J. Betsch, W.B. White. *Spectrochim. Acta, Part A*, **34**, 505 (1978). DOI: 10.1016/0584-8539(78)80047-6
- [50] D. Voll, A. Beran, H. Schneider. *Phys. Chem. Minerals*, **33**, 623 (2006). DOI: 10.1007/s00269-006-0108-8
- [51] M. Chen, D.B. Tanner, J.C. Nino. *Phys. Rev. B*, **72**, 054303 (2005). DOI: 10.1103/PhysRevB.72.054303
- [52] W. Lewis, J.L. Payne, I.R. Evans, H.T. Stokes, B.J. Campbell, J.S.O. Evans. *J. Am. Chem. Soc.*, **138**, 8031 (2016). DOI: 10.1021/jacs.6b04947
- [53] R.X. Silva, C.W.A. Paschoal, R.M. Almedia, M. Carvalho Castro Jr., A.P. Ayala, J.T. Auletta, M.W. Lufaso. *Vib. Spectrosc.*, **64**, 172 (2013). DOI: 10.1016/j.vibspec.2012.05.009
- [54] Wei Huang, Binqing Zhu, Huaiying Zhou, Chao hao Hu, Yan Zhong. *Advances in Engineering Research*, **146**, 309 (2018). DOI: creativecommons.org/licenses/by-nc/4.0/
- [55] T.A. Vanderah, I. Levin, M.W. Lufaso. *Eur. J. Inorg. Chem.*, **14**, 2895 (2005). DOI: 10.1002/ejic.200500234
- [56] Yun Liu, Ray Withers, Hai Binh Nguyen, Kim Elliot, Qijun Ren, Zhanghai Chen. *J. Solid State Chem.*, **182**, 2748 (2009). DOI: 10.1016/j.jssc.2009.07.007
- [57] K.B. Tan, C.C. Khaw, C.K. Lee, Z. Zainal, G.C. Miles. *J. Alloys Compd.*, **508**, 457 (2010). DOI: 10.1016/j.jallcom.2010.08.093
- [58] Weicheng Xu, Zhang Liu, Jianzhang Fang, Guangyin Zhou, Xiaoting Hong, Shuxing Wu, Ximiao Zhu, Yun Fang Chen, Chaoping Cen. *Int. J. Photoenergy*, **2013**, Article ID 394079. DOI: 10.1155/2013/394079
- [59] A.B. Medvedev, R.F. Trunin, *UFN*, **182**, 829 (2012) (in Russian).
- [60] K.A. Aleksandrov, A.T. Anistratov, B.V. Beznosikov, N.V. Fedoseeva, Fazovyie perekhody v kristallakh galoidnykh soedineniy AVKhZ (Nauka, Novosibirsk, 1981), p. 265 (in Russian).
- [61] G. Samara, D. Sakudo, R. Yoshimitsu. *Phys. Rev. Lett.*, **35**, 1767 (1975). DOI: 10.1103/PhysRevLett.35.1767
- [62] J.T. Schick, Lai Jiang, Diomedes Saldana-Greco, A.M. Rappe. *Phys. Rev. B*, **89**, 195304 (2014). DOI: 10.1103/PhysRevB.89.195304
- [63] L.V. Udod, S.S. Aplesnin, M.N. Sitnikov, O.B. Romanova, M.N. Molokeev. *J. Alloys Compd.*, **804**, 281 (2019). DOI: 10.1016/j.jallcom.2019.07.020

Translated by Y.Alekseev